Expression, Purification, and Crystal Structure Determination of Recombinant Human Epidermal-Type Fatty Acid Binding Protein[†,‡]

Carsten Hohoff,[§] Torsten Börchers,[||] Bernd Rüstow,[⊥] Friedrich Spener,*[,§] and Herman van Tilbeurgh[#]

Institut für Biochemie, Westfälische Wilhelms-Universität Münster, Wilhelm-Klemm-Strasse 2, D-48149 Münster, Germany, Institut für Chemo- und Biosensorik, Mendelstrasse 7, D-48149 Münster, Germany, Neonatologische Abteilung, Charité, Humboldt-Universität zu Berlin, Schumannstrasse 20/21, D-10098 Berlin, Germany, and AFMB-UPR 9039 du CNRS, GBMA, 163 Avenue de Luminy, Case 925, F-13288 Marseille, France

Received February 9, 1999; Revised Manuscript Received May 11, 1999

ABSTRACT: We describe the crystal structure of human epidermal-type fatty acid binding protein (E-FABP) that was recently found to be highly upregulated in human psoriatic keratinocytes. To characterize E-FABP with respect to ligand-binding properties and tertiary structure, we cloned the respective cDNA, overexpressed the protein in *Escherichia coli* and purified it to homogeneity by a combination of ion-exchange and size-exclusion chromatographic steps with a yield of 30 mg/L broth. The purified protein revealed a 5-fold higher affinity for stearic acid than for oleic and arachidonic acids. The crystal structure of recombinant human E-FABP was determined to 2.05 Å and refined to an R_{factor} of 20.7%. The initial residual electron density maps clearly showed the presence of a ligand, which was identified as endogenous bacterial fatty acid. Within a central cavity of 252 Å^3, this ligand is bound in a U-shaped conformation, its carboxyl group interacting with tyrosine 131 and arginines 129 and 109, the latter via an ordered water molecule. The E-FABP crystal structure is unique in the FABP family because of the presence of a disulfide bridge between cysteines 120 and 127 that may be physiologically as well as pathophysiologically relevant. Cysteines 67 and 87 are also in close vicinity but in contrast do not form a disulfide bridge. We postulate that this protein belongs to a particular FABP subfamily whose members share common structural as well as functional features.

Long-chain fatty acids were traditionally regarded as building blocks for membranes and as metabolic fuels, but in recent years they have been also recognized as molecules involved in cellular signaling affecting differentiation, regulation of growth, and gene expression (*1*). Thus, at the transcriptional level nuclear receptors of the peroxisome proliferator-activated receptor type are activated by interactions with long-chain fatty acids and facilitate the expression of gene products involved in lipid metabolism and transport of fatty acids across the plasma membrane and through the aqueous compartment of the cell (*2*). Taking part in these intracellular events are the 14−15 kDa fatty acid binding proteins (FABPs). Tertiary structures of this protein family known up to date reveal a highly conserved folding motif, i.e., a β-barrel forming the binding cavity and consisting of two orthogonal β-sheets with five antiparallel β-strands each and an α-helix-turn-α-helix domain partly covering the cavity (*3*). The ligand is noncovalently bound inside the internal central cavity and is almost inaccessible to the solvent.

The human epidermal-type (E-) FABP[1] was originally detected in and cloned from keratinocytes of patients suffering from psoriasis, a hyperproliferative skin disease characterized by abnormal differentiation and disordered lipid metabolism (*4*). Expression levels are greatly enhanced in this pathological situation and E-FABP, the product of the gene FABP5,[2] was immuno-histochemically localized mainly in differentiated keratinocytes (*5*). Interestingly, the protein turned out to be identical to a potent "melanogenic inhibitor" isolated from grafted human skin (*6*), which was shown to inhibit not only tyrosinase activity in normal melanocytes and in a melanoma cell line, but also to reduce cellular proliferation of these cells when added exogenously, while normal skin fibroblasts were unaffected (*7*).

[†] This work was supported by a grant of the Deutsche Forschungsgemeinschaft (Sp 135/10-1).

[‡] The atomic coordinates for the human E-FABP crystal structure have been deposited with the Brookhaven Protein Data Bank (ID code 1b56).

* To whom correspondence should be addressed. Phone: +49 251 83−33100. E-mail: spener@uni-muenster.de. Fax: +49 251 83−32132.

[§] Westfälische Wilhelms-Universität Münster.

[||] Institut für Chemo- und Biosensorik.

[⊥] Humboldt-Universität zu Berlin.

[#] AFMB-UPR 9039 du CNRS.

[1] Abbreviations: A-FABP, adipocyte-type fatty acid binding protein; B-FABP, brain-type fatty acid binding protein; E-FABP, epidermal-type fatty acid binding protein; H-FABP, heart-type fatty acid binding protein; I-FABP, intestinal-type fatty acid binding protein; ILBP, ileal lipid binding protein; M-FABP, myelin-type fatty acid binding protein also known as myelin protein 2; pI, isoelectric point; B_{max}, maximal number of binding sites; K_D, dissociation constant; GC, gas chromatography; RMS, root-mean-square; VDW, van der Waals; MALDI-MS, matrix-assisted laser desorption/ionization mass-spectrometry.

[2] According to the HUGO/GDB Nomenclature Committee, approved gene symbols are on-line available via http://bioinfo.weizmann.ac.il/cards.

10.1021/bi990305u CCC: $18.00
Published on Web 09/03/1999

It is widely accepted that the ability to specifically bind a particular ligand is determined by the three-dimensional structure of a protein. The ability to identify the effect of a particular ensemble of residues on binding affinity would make possible, e.g., the rational design of future drug compounds that will or will not bind with high specificity to a particular FABP type, or even the design of FABPs engineered for a given pharmaceutical ligand. No data on the tertiary fold of E-FABP, one of the most recently discovered and probably most widely expressed members of the FABP family, was available. We were especially interested in the role of the six cysteines, a number unusually high for members of the FABP family, for the three-dimensional structure and in the fatty acid binding mode. To address these questions, human E-FABP was heterologously expressed in *Escherichia coli*, purified and crystallized.

EXPERIMENTAL PROCEDURES

Materials. All chemicals used were of analytical grade and from Sigma (Deisenhofen, Germany), unless otherwise stated. DNA restriction and modification enzymes were purchased from Boehringer Mannheim, Mannheim, Germany. For PCR, a Trio Block thermal cycler (Biometra, Göttingen, Germany) and *Pfu* DNA polymerase (Stratagene, Heidelberg, Germany) were used. Oligonucleotides were purchased from MWG Biotech (Ebersberg, Germany). Molecular cloning procedures followed standard protocols (*8*). Sequencing of double-stranded plasmid DNA was carried out using a DIG Taq Sequencing Kit (Boehringer Mannheim) and direct blotting onto nylon membrane with the GATC 1500 system (GATC, Konstanz, Germany) followed by colorimetric detection. For all chromatographic steps, an FPLC system (Pharmacia, Freiburg, Germany) was used at room temperature with column materials from the same supplier.

Molecular Cloning of Human E-FABP and Expression in E. coli. mRNA was isolated from human mammary gland (divided into a skin and a subcutaneous fat fraction) with the aid of the QuickPrep mRNA Purification Kit and reversely transcribed employing the First-Strand cDNA Synthesis Kit (both Pharmacia) and oligo-d(T) priming. The coding region of the human E-FABP cDNA was amplified with two primers derived from the nucleotide sequence for the cDNA of the protein from psoriatic keratinocytes (*4*). The upstream primer (5′-GCACCCACCATGGCCACA-3′) contained an *Nco*I restriction site and the downstream primer (5′-GTGATGATGGATCCTTTATTCTA-3′) a *Bam*HI restriction site (underlined) for subsequent cloning into the expression vector. PCR was performed with 35 cycles at melting, annealing and extension temperatures of 94 (1 min), 44 (1.5 min), and 72 °C (2 min), respectively, with a final elongation at 72 °C for 10 min. The 431 bp PCR product was cloned into the pCRII vector (Invitrogen, Leek, The Netherlands) to give pCRIIhE-FABP which was subjected to double stranded sequencing. The *Nco*I/*Bam*HI fragment of pCRIIhE-FABP was subcloned into the expression plasmid pET3d (Novagen, Madison, WI) to yield pEThE-FABP, which was used to transform *E. coli* BL21(DE3) (*9*). For production of human E-FABP recombinant *E. coli* were grown in 2 × TY medium (*8*) until OD_{600} reached 0.6−1.0 and induced with 0.4 mM (final concentration) isopropyl-β-D-thiogalactopyranoside (MBI Fermentas, St. Leon-Rot, Germany). Rifampicin was added 45 min later to a final concentration of 175 μg/mL (*9*). The cells were harvested after 16 h by centrifugation (5000*g*, 15 min, 4 °C), resuspended in a 3-fold volume of 10 mM Tris-HCl, pH 7.4, containing 20 units Benzonase (Merck, Darmstadt, Germany) and disrupted by sonication (3 × 10 s, 20 W, 0 °C). After addition of 1.5% (w/v) streptomycin sulfate (final concentration), a cleared lysate was obtained by centrifugation (28000*g*, 45 min, 4 °C) and desalted on Sephadex G-25 (5 × 20 cm, 5 mL/min), equilibrated in 10 mM Tris-HCl, pH 7.4. Pooled protein containing fractions, as monitored by the Bradford assay, were applied to a Q-Sepharose Big Beads column (5 × 20 cm, 5 mL/min) and eluted by a gradient of 1 M NaCl in 10 mM Tris-HCl, pH 7.4. E-FABP-containing fractions, identified by SDS−PAGE according to Laemmli (*10*), were pooled, concentrated by ultrafiltration (Amicon, Witten, Germany), and finally applied to a Superdex 75 column (1 × 60 cm, 1 mL/min) equilibrated in phosphate-buffered saline (PBS, 10 mM sodium phosphate and 154 mM NaCl, pH 7.4). Recombinant human E-FABP (1 mg/mL) was delipidated by incubation with Lipidex-1000 (Canberra Packard, Dreieich, Germany), suspended as 50% (w/v) slurry in 20 mM Tris-HCl (pH 8.0), for 1 h at 37 °C with occasional mixing. The concentration of human E-FABP was determined spectrophotometrically based on the content of aromatic amino acids using $A_{280}(1\%) = 9.7$ (*11*). Isolelectric focusing was done with the Pharmacia PhastGel system using precast PhastGel IEF gels (pI range 3−9) and pI markers (broad pI kit, pH 3.5−9.3) according to the manufacturer's instructions.

Ligand-Binding Studies. The Lipidex assay was performed according to the modification introduced by Xu et al. (*12*). Briefly, delipidated recombinant human E-FABP (0.5 μM) was at least in duplicate incubated with different concentrations (up to 12 μM) of 1-^{14}C-fatty acids with a specific activity of 53−55 Ci/mol (Amersham, Braunschweig, Germany) in binding buffer (20 mM Tris-HCl, and 0.1 mM Triton X-100, pH 8.0) at 37 °C for 15 min. The assay solution was chilled on ice and applied to a 2 mL Lipidex column at 4 °C, and the fatty acid/FABP complex was eluted with binding buffer, while fatty acids not bound to E-FABP were eluted with 3 mL of methanol. The radioactivity of both fractions was measured by liquid scintillation counting (LKB 1219 Rackbeta, LKB, Freiburg, Germany) and provided the values for bound and unbound ligand, respectively. After correction for a blank (i.e., buffer without protein), the binding constants B_{max} and K_D were determined by nonlinear regression (SigmaPlot, Jandel Scientific, Erkrath, Germany) fitting the following model to the data

$$B = B_{max}F/(K_D + F)$$

where F is unbound fatty acid concentration and B is bound fatty acid concentration.

Typically, the blank was below 10% of the radioactivity applied.

Thiol Titrations. Purified human E-FABP was incubated with a 20-fold molar excess of 5,5′-dithiobis(2-nitrobenzoate) in 50 mM Tris-HCl, pH 8.0, containing 10% (w/v) sodium dodecyl sulfate as denaturant. The thionitrobenzoate dianion liberated was monitored with a Shimadzu UV-2100 spec-

trophotometer, and the number of free cysteines was quantified using an absorption coefficient of 13 700 M^{-1} cm^{-1} at 412 nm (*13*).

Analysis of Endogenous Ligands. Recombinant E-FABP and the *E. coli* BL21(DE3) cells used as expression hosts were extracted with chloroform/methanol (2:1, v:v) after addition of C_{17} margaric acid as internal standard. Fatty acids extracted were esterified with trimethylsulfonium hydroxide (Macherey−Nagel, Düren, Germany) in the injector of the gas chromatograph at 250 °C. The resulting methyl esters of fatty acids were analyzed with the aid of a Shimadzu GC-10A gas chromatograph equipped with a FS-FFAP column (25 m × 25 mm) (Macherey−Nagel). Helium served as carrier gas, while hydrogen and synthetic air (all gases from Westfalen, Münster, Germany) were used for the flame-ionization detector, which was maintained at 250 °C. The column temperature was held at 80 °C for 1 min, then increased to 180 °C at 15 °C/min, and further at 5 °C/min on to 220 °C, which was maintained for 20 min. Fatty acid methyl esters were identified by comparison of their retention times with those of known standards. Identification was verified by applying gas chromatography−mass spectrometry.

Analysis of Primary Structure. After dialysis against 10 mM ammonium acetate (pH 7.0) and lyophilization, N-terminal sequence analysis of recombinant human E-FABP was carried out with a pulsed liquid sequenator (model 477A) equipped with a 120 A PTH analyzer (both from Applied Biosystems, Weiterstadt, Germany).

The molecular mass of recombinant human E-FABP, dialyzed against 10 mM HEPES (pH 7.4), was measured by matrix-assisted laser desorption/ionization mass-spectrometry (MALDI-MS), essentially as described earlier (*14*). At least three mass determinations were done with horse cytochrome *c* (12 360.1 Da) and horse *apo* myoglobin (16 952.5 Da) serving for mass calibration.

Crystallization and Structure Determination. The protein was kept for storage in PBS since a physiological ionic strength was mandatory for maintenance of a folded protein. NMR analyses of samples without salt have shown that the protein was principally unfolded (data not shown). Crystals were obtained by the vapor diffusion hanging drop method. Initial conditions were obtained by the sparse matrix grid screen (Hampton Research). One microliter of protein was mixed with 1 μL of well solution containing 2 M $(NH_4)_2SO_4$, 0.2 M sodium/potassium-tartrate, and 0.1 M citrate buffer, pH 5.6. Small crystals were obtained at room temperature, which grew slowly over a few weeks to a final size of 400 × 400 × 200 μm^3. The initial diffraction data of the crystals were measured on a RIGAKU rotating anode, equipped with a MAR research phospho-imaging detector and the space group was determined as $P4_32_12$ or $P4_12_12$ ($a = b = 63.5$ Å, $c = 76.7$ Å). A complete data set at 2.8 Å was collected at room temperature by 1° oscillations (native data set I). Data statistics are gathered in Table 1. Further data reduction used the CCP4 chain of crystallographic programs (*15*).

The structure was solved by molecular replacement as implemented in the AMORE package (*16*) using data set I. As a starting model we used the *holo* human heart-type (H-) FABP structure (*17*) in which all the nonidentical residues were replaced by alanine. H-FABP has 48% strict sequence identity and 65% of the residues are similar to human E-FABP. The translation function showed a very clear solution for the $P4_32_12$ spacegroup option. Rigid refinement of the molecular replacement solution model yielded a correlation coefficient of 34% and a 50.7% R_{factor}. The validity of the molecular replacement solution was confirmed on the graphics screen by a good crystallographic packing arrangement. All molecular graphics manipulations used the crystallographic modeling program TURBO (*18*).

Table 1: Parameters for Resolution of the 3D Structure

	native data set I	native data set II
R_{merge} (%)[a]	9.8	7.0
resolution range (Å)	2.8	2.05
no. of observations	27 096	72 226
no. of unique reflections collected	4204	10 321
completeness (%)	99.5	99.7
$I/\sigma(I)$ at outer shell	11	12

[a] $R_{merge} = \Sigma|I_i - I_m|/\Sigma I_m$, where I_i and I_m are the observed intensity and mean intensity of related reflections.

A high-resolution data set (set II, Table 1) for refinement was collected on the DW32 synchrotron beam line at LURE (Paris). Ninety 1° oscillation images were collected at room temperature using the MAR research detector ($\lambda = 0.97$ Å). Data reduction used the DENZO package and scaling was done with SCALEPACK (*19*). A complete data set at 2.05 Å resolution was obtained ($R_{merge} = 7\%$). A summary of these data collection can be found in Table 1.

The model was completed and refined using data between 6.0 and 2.05 Å resolution by iterative cycles of model building and simulated annealing refinement using X-PLOR version 3.1 (*20*). The progress of the refinement was evaluated by the R_{free} factor (calculated for 7% of the reflections never used in the refinement). After refinement of the protein model to an R_{factor} of 24% ($R_{free} = 29\%$), an elongated and continuous stretch of residual well-defined $2F_o - F_c$ electron density was observed in the cavity of the molecule, which is known to bind the fatty acid ligands in the other members of the FABP family. Although no extra fatty acids were included during the crystallization trials, biochemical analysis of the purified recombinant protein showed that it had a mixture of endogenous bacterial fatty acids bound. No fatty acid analysis was carried out on the crystals, but the shape and the length of the density clearly indicated the presence of a C_{16} or C_{18} type fatty acid. Therefore, palmitic acid was modeled into the electron density and apparent water molecules were added. The occupancy of the ligand was set to a constant value of 0.5 and B_{factor}s refined to values comparable to those of the surrounding side chains. The final refinement yielded an $R_{factor} = 20.7\%$ ($R_{free} = 26.5\%$) and good stereochemistry (Table 2).

RESULTS

Characterization of Recombinant Human E-FABP. The E-FABP cDNA cloned from both mammary gland fractions (skin and subcutaneous adipose tissue) was found to be 100% identical (data not shown) to the E-FABP cDNA from psoriatic keratinocytes originally described by Madsen et al. (*4*). It is noteworthy that despite the presence of six cysteines recombinant human E-FABP was expressed as a soluble

Table 2: Refinement Statistics

total non-H atoms	1101
ligand atoms	18
water sites	51
data range (Å)	6.0−2.05
number of reflections used for refinement	9509
R (%)[a]	20.7
R_{free} (%)[b]	26.5
RMS deviations	
bonds (Å)	0.01
angles (deg)	1.79

[a] $R = \Sigma|F_{obs} - F_{calc}|/\Sigma F_{obs}$ for the remaining 90% of the data included in the refinement. [b] $R_{free} = \Sigma|F_{obs} - F_{calc}|/\Sigma F_{obs}$ for 10% of data randomly selected and excluded from the refinement.

protein in *E. coli* at 37 °C in contrast to murine B-FABP, that contains five cysteines and was expressed as inclusion bodies at this temperature (*21*). By inhibiting bacterial RNA polymerases with rifampicin during expression, the yield was considerably increased (typically 30 mg/L broth). Most of the bacterial proteins were removed in the anion exchange chromatography step (Figure 1), where recombinant E-FABP eluted early in the salt gradient (at 120 mM NaCl). After the final gel filtration, the protein was homogeneous as judged from SDS−PAGE (data not shown). Isoelectric focusing of recombinant human E-FABP under native conditions revealed two isoforms with pI values of 6.2 and 6.4 (Figure 1, inset). The more basic isoform was at least twice as intense as the acidic isoform.

N-Terminal sequencing after automated Edman degradation revealed the amino acid sequence Ala-Thr-Val-Gln-Gln-Leu-Asn-Gly-Arg-Trp. The molecular mass of human E-FABP derived from collinear cDNA is 15 164 Da, without the first methionine 15 033 Da. By MALDI-MS, the molecular mass was determined to 15 027 ± 5 Da, which is very close to the value for E-FABP without the first methionine. A small peak shoulder in the mass spectrum at 15 192 ± 7 Da can be explained by the presence of unprocessed, formylated recombinant E-FABP (starting with fMet-Ala-Thr-Val-Gln-Gln-Leu-Asn, molecular mass 15 193 Da). Since the N-terminus of this isoform is blocked, it would remain undetected by Edman degradation as reported for recombinant bovine heart-type FABP (*14*).

By application of Ellman's assay, the number of cysteines of denatured recombinant human E-FABP was determined to 3.6 ± 0.2 ($n = 3$). This led us to assume one intramolecular disulfide bridge in the recombinant protein since the cDNA encodes six cysteines.

Binding of Fatty Acids. GC analysis revealed that purified recombinant human E-FABP was associated with *E. coli* long-chain fatty acids. Approximately 60% of E-FABP was present as *holo* protein with palmitoleic acid as major ligand (48.9 mol %). *cis*-Vaccenic acid (28.8 mol %), palmitic acid (17.3 mol %), and a long-chain cyclopropylic fatty acid (5.8 mol %), which represents a new, naturally occurring ligand for members of the FABP family resembling a cis-unsaturated fatty acid, were other ligands identified (Table 3).

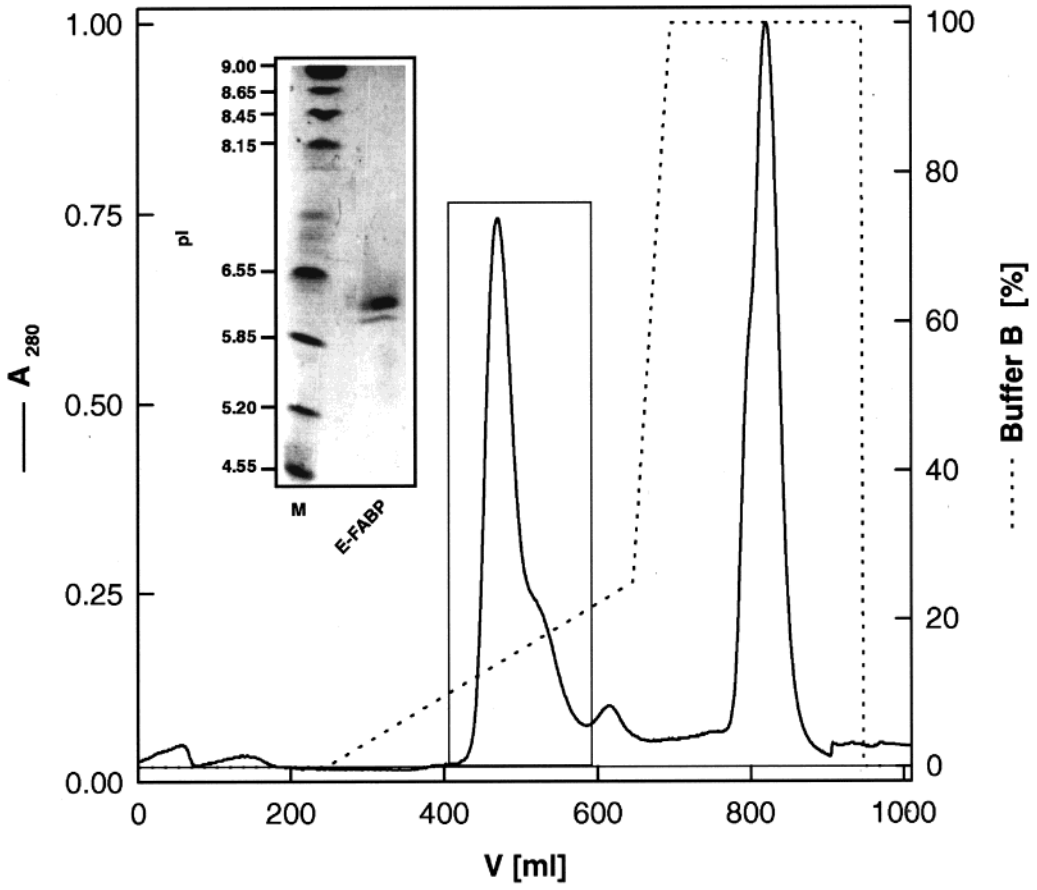

FIGURE 1: Anion-exchange chromatography on Q-Sepharose BB (20 × 5 cm, 5 mL/min) as most effective step in the course of purification of recombinant human E-FABP (pooled fractions boxed). Buffer B, 1 M NaCl in 10 mM Tris-HCl (pH 7.4). (Inset) Microheterogeneity of recombinant human E-FABP (2 μg). Native isoelectric focusing was performed with PhastGel IEF gels (pI range 3−9) and pI markers (broad pI kit, pH 3.5−9.3, M).

Table 3: Composition of Fatty Acids Extracted from Recombinant Human E-FABP and from the Respective *E. coli* Expression Strain

	mol %	
fatty acid[a]	recombinant human E-FABP	*E. coli* BL21(DE3)
12:0	0	1.5
14:0	0	4.5
16:0	17.3	41.0
17:0	0	1.1
18:0	0	0.9
16:1[b]	48.9	4.5
18:1[c]	28.8	13.1
cyclo-17[d]	5.8	22.5
cyclo-19[e]	0	7.5

[a] No. of carbon atoms: number of double bonds. [b] Palmitoleic acid (*cis*-9-hexadecenoic acid). [c] *cis*-Vaccenic acid (*cis*-11-octadecenoic acid). [d] *cis*-9,10-Methylenehexadecanoic acid. [e] *cis*-9,10-Methyleneoctadecanoic acid. Given are the means of three determinations with a standard deviation below 10%.

Comparison of the fatty acid composition of the expression strain and the recombinant human E-FABP reveals an enrichment of palmitoleic acid (10-fold) and *cis*-vaccenic acid (2.5-fold), while palmitic acid (2.5-fold) and *cis*-9,10-methylenehexadecanoic acid (4-fold) are reduced (Table 3).

On the basis of the Lipidex binding assay, saturated stearic acid was the preferred ligand ($K_D = 0.29 \pm 0.06$ μM, $B_{max} = 0.8 \pm 0.1$) for delipidated recombinant human E-FABP, while monounsaturated oleic acid and polyunsaturated arachidonic acid were bound with lower affinities ($K_D = 1.6 \pm 0.2$ μM, $B_{max} = 0.54 \pm 0.11$ and $K_D = 1.73 \pm 0.25$ μM, $B_{max} = 0.53 \pm 0.15$, respectively).

Resolution of the Structure and Quality of the Model. As could be expected from the sequence analogy with other members of the FABP family, the 3D structure of E-FABP is a typical member of the 10 stranded β-clam structure group. Its backbone structure is virtually identical to that from, e.g., H-FABP (*47*) or I-FABP (*22*). Root-mean-square (RMS) deviations in Cα positions (Figure 2) after superposition of the structures are 0.62 Å with H-FABP (115 residues) and 1.03 Å with I-FABP (93 residues), reflecting the phylogenetic relationship (Figure 5C).

The final model contains 1101 protein atoms, 16 ligand atoms, and 51 waters. The model has good stereochemistry (Table 2), and 99.2% of the residues are in the allowed Ramachandran regions. The vast majority of the residues has well-defined electron density. There are, however, two problematic regions. First, only very weak and interrupted density was observed for the first three residues (starting with the N-terminal methionine). Interpretation of the weak density did not lead to a consistent model, and therefore, these N-terminal residues are not included in the final model. The other less defined region is the loop between strands C and D, comprising residues 59−61. Introducing the conformation of this loop as observed in the H-FABP structure, which was used for solving the molecular replacement, did not give a satisfactory result during refinement. This loop probably adopts two or more conformations in the crystal. Rebuilding of the loop and subsequent refinement with a 50% occupancy, however, did not yield sufficiently good $2F_o - F_c$ maps to allow construction of other conformers. This region in FABPs interacts with the aliphatic end of bound fatty acids and is called the portal region because it is believed that the fatty acid enters/exits the cavity at this region (*23*). Multiple conformations of this loop may be related to the partial occupancy of the bound fatty acid (see further). This loop contains Val60, which is a phenylalanine in most other FABP sequences (Figure 5B) and which is thought to affect dynamics of lipid exchange with the exterior (*24*). At this position, also the orthologs of human E-FABP, detected in rat skin (*25*), lens (*26*), and nervous system (*27*), in mouse squamous cell carcinoma (*28*) as well as in adipocytes (*29*), and lens (*30*), retina, and testis (*31*) from cattle, have a smaller but hydrophobic residue as can be seen in Figure 5A. For a better visualization of the phylogenetic relationships, a radial rootless tree is shown in Figure 5C.

A remarkable difference between the amino acid sequence of human E-FABP, compared with the other paralogous FABPs, is the presence of six cysteines. Four of them are unique to the E-FABP (Cys43, Cys47, Cys67, and Cys87). Some FABPs have one or two cysteines homologous to the E-FABP Cys120 and/or Cys127 (but only M-FABP has both, Figure 5B). The folding of the protein approaches two Cys couples close to each other in the 3D structure: Cys67/Cys87 and Cys120/Cys127. This would in principle allow the formation of two Cys bridges. We therefore compared during the initial stages of the refinement the results obtained with

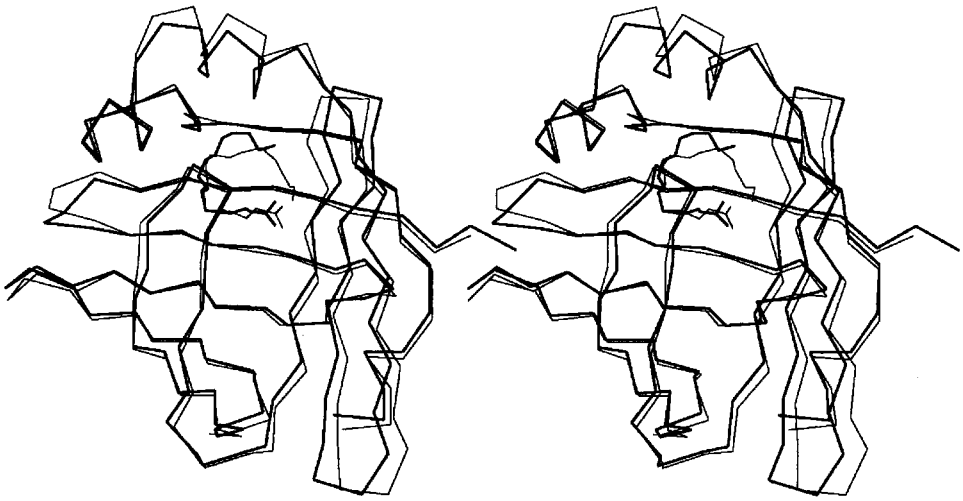

FIGURE 2: Stereodiagram of the Cα superposition of the E-FABP (thick line) and the H-FABP (thin line) 3D structures. The H-FABP structure (*47*) was used as initial model for solving the molecular replacement.

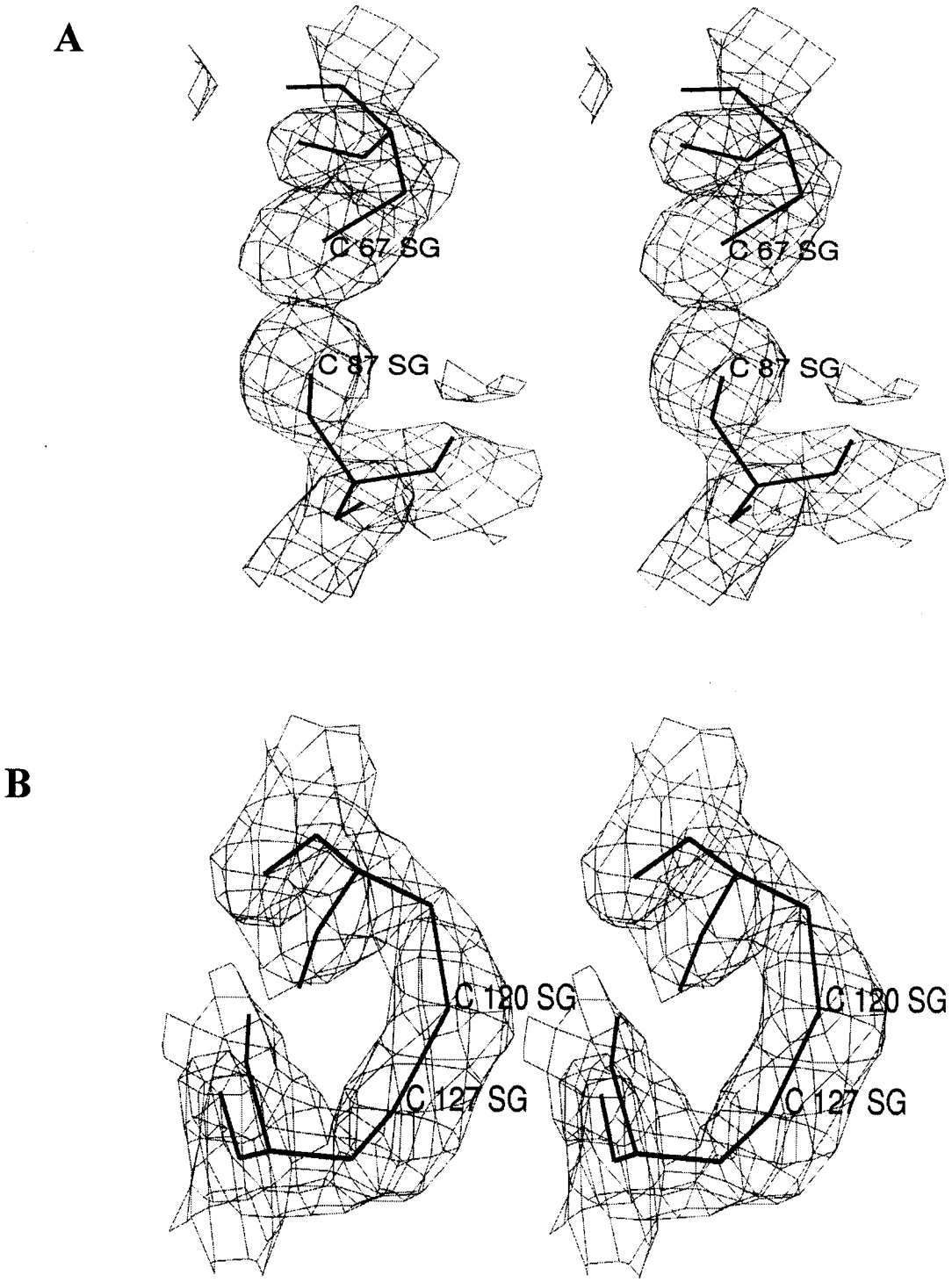

FIGURE 3: Stereoview of the final $2F_o - F_c$ residual electron density map, contoured at the 1σ level, around two couples of cysteines: Cys67/Cys87 (A) and Cys120/Cys127 (B).

two different models: one with and one without imposing the two disulfide bridges. The molecular replacement model only contained Ala side chains at the Cys positions, and after the first refinement cycle, the Cys side chains could be unambiguously placed into the $2F_o - F_c$ electron density. Further refinement showed a negative peak at the 3σ level between the sulfur atoms of Cys67 and Cys87 in the $2F_o - F_c$ electron density when the two disulfides were imposed. The density map around the Cys120/Cys127 disulfide bridge did not show any negative nor positive residual electron density features and seemed to envelop perfectly the imposed disulfide bridge. We therefore removed the disulfide bond between Cys67 and Cys87 in the next refinement round. This resulted in an improved R_{free} factor, rubbing out the negative and positive residual electron density features around these two cysteines (Figure 3). The remaining two cysteines (Cys43 and Cys 47) are too far removed in the 3D structure from any other cysteine partner to be engaged in a disulfide bridge. Cys43 contacts the acidic headgroup of the bound ligand via a water molecule. We can therefore conclude on crystallographic grounds that the E-FABP contains one disulfide bridge between Cys120 and Cys127, which is in agreement with biochemical results showing the presence of a single disulfide bridge.

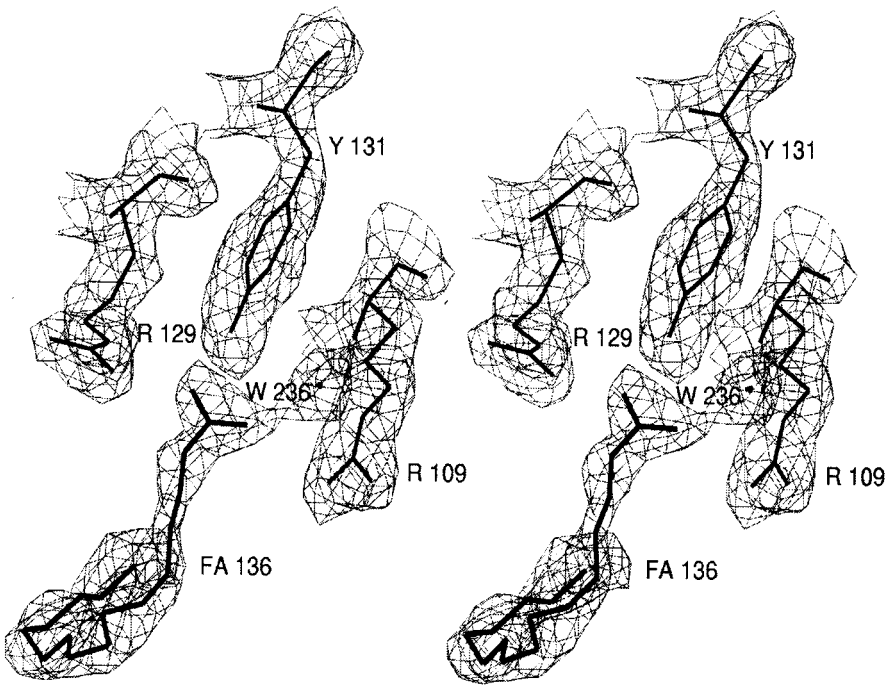

FIGURE 4: Detailed stereoview of fatty acid binding. The bound fatty acid is in thick and the contacting residues are in thin lines. The $2F_o - F_c$ electron density is equally represented at the 1σ level.

It is not clear why Cys67 and Cys87 do not form a disulfide bond, although nothing apparent prevents them from doing so. This disulfide would bridge strands D and F. One of the main characteristics of the disulfide bridge is the dihedral angle around the S−S bond (χ_3). The tentative model of a Cys67−Cys87 disulfide bridge (which resulted in strong negative and positive peaks in the residual electron density maps) yielded a value for $\chi_3 = 137°$, which did not correspond to the frequently observed left ($\chi_3 = -90°$)- or right ($\chi_3 = 90°$)-handed spiral structure (*32*, *33*). The majority of nonlocal disulfides adopts the left-handed spiral structure. The distance between Cα atoms is 7.3 Å, which is between the observed range for disulfides (4.6−7.4 Å). The value for the χ_3 angle in the modeled FABP bridge is rare but not exceptional since it is for instance observed in the immunoglobulin family. The χ_2 distribution of disulfides is very broad and therefore not very discriminative. The remaining torsion angles of the imposed disulfide bridge ($\chi_1 = 106°$, $\chi_2 = -176°$, $\chi_2' = 142°$, $\chi_1' = 22°$) are also rather remote from what is usually observed. The Cys120/Cys127 bridge has the following torsion angles: $\chi_1 = 58°$, $\chi_2 = -51°$, $\chi_3 = 130°$, $\chi_2' = 112°$, $\chi_1' = 80°$ and a Cα−Cα distance of 4.7 Å. These values are closer to but still different from the right-handed spiral configuration.

Sequence similarity with other members of the FABP family suggested that E-FABP could bind lipophilic molecules with an acidic headgroup as well, which was experimentally verified (*34*). Before refinement of the protein structure, the initial electron density maps already indicated that there was a ligand bound inside the barrel. A strong and elongated $2F_o - F_c$ electron density could accommodate one fatty acid with a chain length of C_{16} or C_{18}. A palmitic acid was fitted into the density. Including the ligand during the refinement improved the R_{free} factor. The B_{factor}s of the ligand (full occupancy) refined to a global value of about 42 Å^2. This value is higher than those for most of the side chains inside the barrel and those for some internal well-fixed water molecules. Refinement with a fixed 50% occupancy of the ligand yielded B_{factor}s comparable with those of surrounding protein side chains and waters. The shape of the electron density did not allow determination of the presence of double bonds in the bound ligand. Saturated and unsaturated fatty acids bind for instance in a very similar way in the case of the I-FABP. We modeled a saturated fatty acid into the density to allow for more conformational freedom, but an unsaturated fatty acid could be introduced without any problem. GC analyses revealed that fatty acids with a C_{16} acyl chain (hexadecanoic, *cis*-9-hexadecenoic and *cis*-9,10-methylenehexadecanoic acids, respectively) represent nearly two-thirds of the fatty acids associated with recombinant human E-FABP (Table 3). After refinement some elongated residual density emanating from the lipid chain C5 carbon stretched out to the Tyr131 OH group. Maybe this indicates some alternative binding mode with low occupancy. The program VOIDOO (*35*) was used to delineate the cavity and assess its volume to 252 Å^3, which is very close to the value for H-FABP (260 Å^3).

As can be observed from Figure 4, the interactions of E-FABP with the bound fatty acid are very similar to those observed for other FABP complexes (*3*). The carboxylic headgroup forms salt bridges with Arg109 and Arg129 and a direct hydrogen bond with Tyr131 OH. The first part of the aliphatic chain is in van der Waals (VDW) contact with a number of strongly bound water molecules, while from C9 on more hydrophobic VDW contacts are prevailing (Met23, Met35, and Gly36).

DISCUSSION

The overall X-ray structure of human E-FABP depicted in Figure 6 is very similar to M-FABP [also known as myelin P2 (*36*)], A-FABP (*37*), or H-FABP (*38*). For instance, the RMS deviation between Cα positions for 115 residues

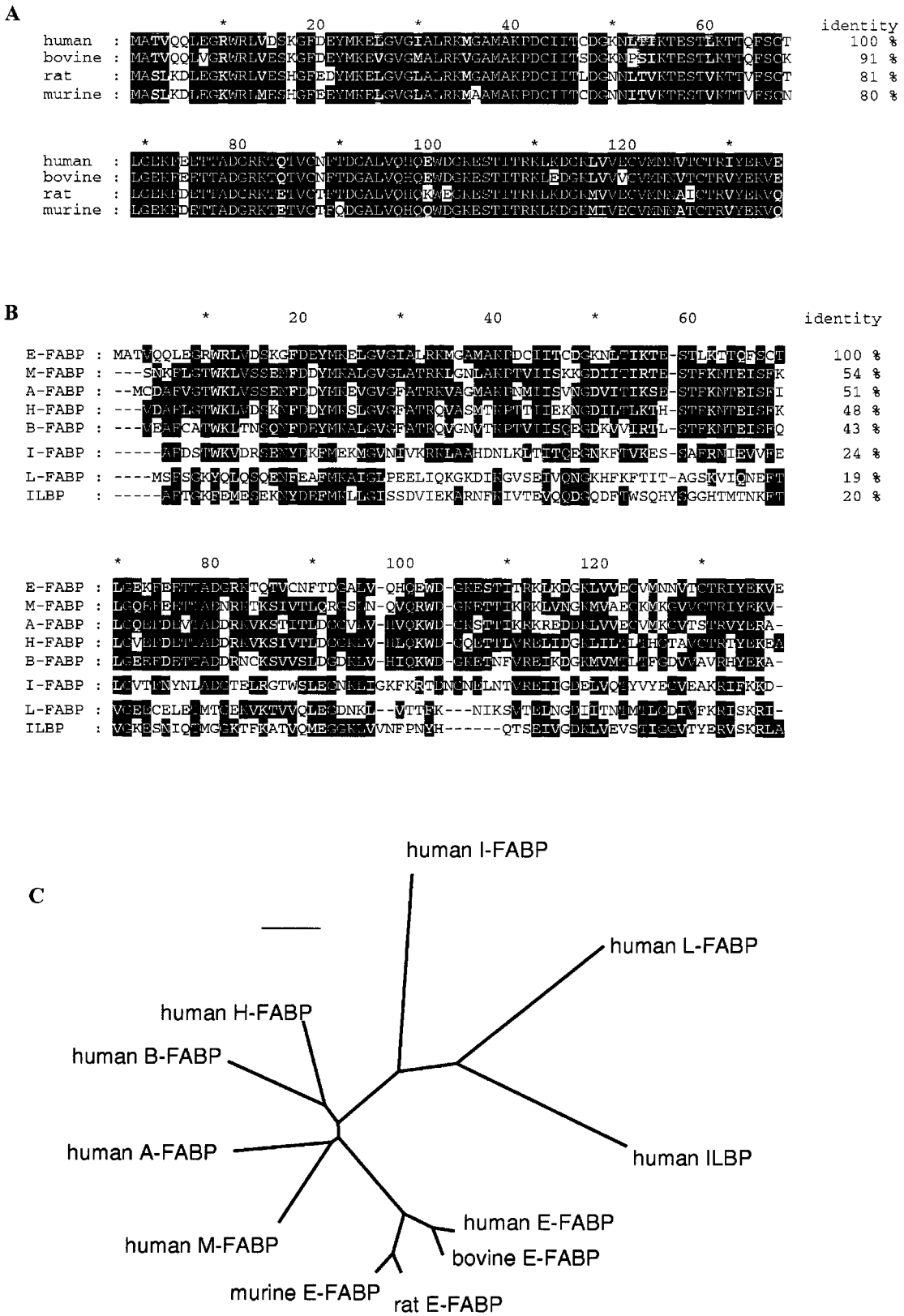

FIGURE 5: Amino acid alignment of E-FABP orthologs (A) and paralogs (B). Sequences were aligned using CLUSTAL W (implemented in the HUSAR 5.0 package, DKFZ Heidelberg, Germany) and displayed with GeneDoc 2.4.000 [Nicholas, K. B., and Nicholas, H. B., Jr. (1997). Distributed by the authors via http://www.cris.com/~ketchup/genedoc.shtml]. Identical amino acids are shaded black and similar amino acids gray. Subfamilies are separated by a gap. (C) Radial rootless phylogenetic tree of mammalian E-FABP orthologs and paralogs. Subfamily of the cellular retinoid binding proteins (*54*) has been omitted for clarity. Phylogenetic order was calculated with CLUSTAL W and visualized by TreeView (*55*). Branch length represents evolutionary distance between proteins with the scale bar representing a substitution of 10 amino acids. GenBank accession numbers are (human E-FABP) M94856, (bovine E-FABP) U55188, (murine E-FABP) X70100, (rat E-FABP) S69874, (human M-FABP) X62167, (human A-FABP) J02874, (human B-FABP) O15540, (human H-FABP) X56549, (human I-FABP) P12104, (human L-FABP) P07148, (human ILBP) P51161. For a comprehensive phylogenetic tree of FABPs from all phyla see (*56*).

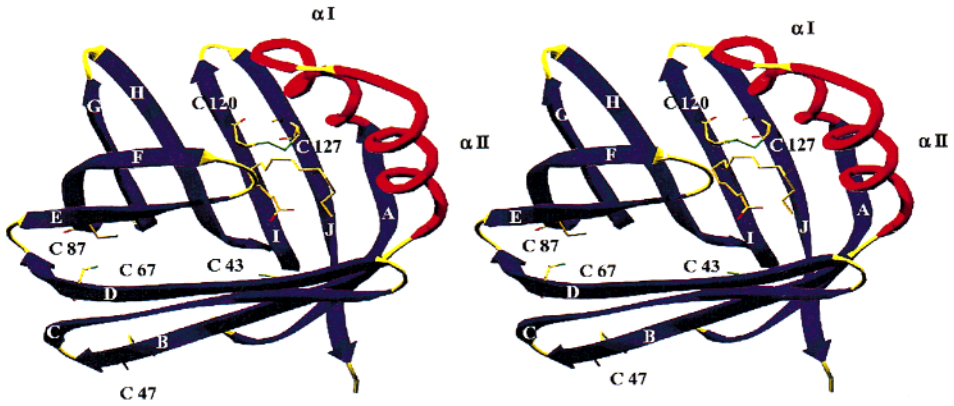

FIGURE 6: Overall ribbon representation of the E-FABP tertiary structure. Bound ligand and the six cysteine residues are represented as stick models (Cys43 is partially hidden behind strands B and C). Figure was generated using SwissPDBViewer 3.1 and PovRay 3.1. The β-strands forming the barrel are consecutively labeled A to J, the helices αI and αII.

between E-FABP and H-FABP is 0.62 Å, and this is in good agreement with the 0.7 Å RMS deviation found for the backbone atoms of the A-FABP and H-FABP high-resolution X-ray structures (*39*). The general structural aspects of fatty acid binding proteins have been amply discussed and reviewed (*3, 40*). For this discussion we will therefore focus on unique aspects of the structure presented here.

A remarkable feature of E-FABP is the presence of one cystine bridge between Cys120 and Cys127. Such a post-translational modification has not been reported for any other fatty acid binding protein. Only few other FABP sequences have cysteine at the equivalent positions. Cys127 seems better conserved than Cys120. M-FABP, purified from bovine caudal spinal root myelin, contains two cysteines at analogous positions (117 and 124), and biochemical results suggested that they form a disulfide bridge (*41*), while the crystallographic structure determination, however, did not confirm this observation. In the final model, the S^{γ} positions are separated by 4.5 Å (*36*). Comparison of the M-FABP and E-FABP structures shows that the main-chain region comprising these two cysteines are superposable and that there are no obvious structural reasons for the different oxidation state of these two cysteines in these two proteins. Cys bridges are not usually present in intracellular, but instead in extracellular proteins. On one hand, E-FABP has been detected as a protein partially externalized by keratinocytes (*4*). The observed function of E-FABP as "melanogenic inhibitor"—if physiological at all—would require a release of E-FABP from keratinocytes and an uptake by melanocytes. It has been reported that keratinocytes produce polypeptides that regulate the phenotype of melanocytes, which donate melanin pigments to neighboring keratinocytes (*42*). Such a physiological disulfide bridge may help stabilizing E-FABP in such an extracellular trafficking. For bovine E-FABP (originally termed "lens protein 2" or lP2), the formation of a disulfide bond under appropriate pathophysiological conditions (e.g., during oxidative stress leading to lens cataract formation) was suggested (*30*). On the other hand, there are some recent reports on the existence of disulfide bonds in cytosolic proteins, e.g., in two members of the S100 multigene family of calcium-binding proteins (*43, 44*).

The E-FABP used in the present study was overexpressed in *E. coli*, whose cytoplasm is not a favorable environment for the oxidation of cysteines. Formation of the disulfide bridge in E-FABP thus may have occurred during the purification procedure under atmospheric oxygen. In recombinant murine E-FABP (originally termed "keratinocyte lipid-binding protein" or MAL-1), all six cysteines were detected (*34*). It is not clear by comparing the purification protocol for recombinant murine E-FABP with that for our recombinant human E-FABP why there should be any difference in the oxidation state of the cysteines. Oleic and arachidonic acid binding protected one to two cysteines in recombinant murine E-FABP against modification. Cys120/Cys127 is close to the bound ligand in the E-FABP structure at the opposite site of the so-called portal region, but it does not seem to interact directly with the bound ligand, nor to impose any particular conformation that would influence ligand interactions of neighboring residues. The influence of this disulfide bridge on the lipid-binding capacities could be tested by site directed mutagenesis.

Structure refinement was carried out using a palmitic acid model, which seemed the best fitting ligand for the observed electron density since the resolution of the diffraction data does not allow unambiguous identification of the nature of the ligand bound inside the central cavity. The shape and the volume of the residual electron density is clearly in favor of a C_{16}- or C_{18}-type fatty acid, which is in accordance with the GC data. There remains uncertainty, however, about (i) the homogeneity of the bound ligand (the presence of a mixture of various analogous ligands in the crystal is possible), (ii) the occupancy of the ligand(s), and (iii) the presence of double bonds in the acyl chain. Since no extra ligand was added in the crystallization liquid, the bound ligand was picked up from *E. coli* either during cytosolic expression or during the cell disruption. We did not perform fatty acid analysis of the protein crystals and it therefore cannot be excluded that the ligand distribution (if any) in the crystals is different from that in solution.

The physiological ligand(s) of E-FABP are unknown. Binding experiments with recombinant murine E-FABP (80% identical and 93% similar to human E-FABP on the level of primary structure) revealed highest affinity for long-chain fatty acids. The affinity slightly decreased with increasing number of double bonds and decreasing chain length (*34*). Recombinant bovine E-FABP (*31*) had highest affinity for palmitic acid, while the affinity for C_{18} fatty acids de-

creased with increasing the number of double bonds (stearic acid was not analyzed). It is interesting to note that—like the recombinant protein—the authentic human E-FABP, isolated from human psoriatic keratinocytes, showed highest affinity for the saturated C_{18} stearic acid, while increasing chain length and degree of unsaturation reduced binding affinity (*5*). It is of vital interest for a cell to have a carrier available for such an important fatty acid that is virtually insoluble in an aqueous environment (*45*). This ligand specificity may be one reason for the widespread expression of E-FABP, for which ESTs[3] are reported for adipose tissue, aorta, brain, mammary gland, esophagus, eye, germ cell, heart, kidney, larynx, lung, placenta, prostate, testis, thyroid, tonsil, and uterus.

During the preparation of this manuscript, a paper describing the heterologous expression and purification of human E-FABP (fused to an N-terminal hexa-histidine tag) has appeared (*46*). In a dialysis binding assay, this His-tagged protein showed multiple binding of fatty acids, especially of medium chain length. Myristic acid was the longest fatty acid assayed with a K_D of 2.3 μM while the other shorter ligands were bound up to 50 times worse. There was no evidence for more than one fatty acid bound in our crystal structure. A direct comparison of the binding parameters is difficult due to different techniques used for the ligand binding studies (including different pH and ionic strength).

The binding mode of the ligand in the E-FABP structure is identical to that observed in M-FABP, H-FABP, and A-FABP complexed to fatty acids (*17*, *24*, *36*, *47*). The bound ligand in E-FABP, which we interpreted as palmitic acid, adopts a U-shaped conformation as observed in protein fatty acid complexes of these three FABPs (Figures 2 and 6). The bend in the E-FABP bound fatty acid is induced by gauche conformations between C6/C7 and C11/C12. The shape, volume, and physicochemical aspects of the lipid-binding cavity of these FABPs are very well conserved and therefore result in almost identical fatty acid binding. The binding mode is clearly distinct from that observed in I-FABP, where the fatty acid adopts a more elongated conformation and occupies a different location. It is also clearly different from the binding modes observed for the two fatty acids which are bound to L-FABP (*48*). One carboxyl oxygen of the fatty acid forms hydrogen bonds with the OH group of Tyr131 and with the Nϵ group from Arg129, two residues which are absolutely conserved in the FABP family. These residues bind identically to the fatty acid in the complexes of M-FABP, H-FABP, and A-FABP. The second carboxyl oxygen is bound to a water molecule, which also forms a second hydrogen bond with Nϵ of Arg109. The association of this carboxyl oxygen is slightly different in H-FABP and A-FABP, where it is bound to a second water molecule, not observed in the E-FABP structure. From molecular dynamics calculations, a protonated fatty acid headgroup has been proposed for the closely related A-FABP and H-FABP, in contrast to the evolutionary more distant I-FABP, for which a charged carboxylate was calculated (*39*). Site-directed mutagenesis of Arg129 or Arg109 in A-FABP results in considerable loss of affinity (*50*). The aliphatic chain of the fatty acid interacts mainly with hydrophobic side chains of the barrel interior: Phe19, Met23, Leu32, Met35, Gly36, and Val118 make one or more van der Waals contacts. This type of contact is equally observed in the complexes of M-FABP, H-FABP, and A-FABP (the majority of the contacting residues are strictly conserved). As the thorough thermodynamic study by Richieri et al. on fatty acid binding to A-FABP and I-FABP mutants have shown, the importance of these individual interactions is very difficult to predict from inspection of the structure alone (*50*). Considering the close resemblance between A-FABP and E-FABP, we may presume that the effect of substitutions in E-FABP will follow the trend observed in A-FABP. Apart from ligand, eight water molecules were identified inside the cavity, some with thermal factors comparable to those of the surrounding protein. Most of these water molecules fill the pocket of the ligand-binding site, surrounded by the bent fatty acid. A few of the water molecules are also situated at VDW distances of acyl carbons (C5, C7, and C8). These water molecules are all bound to hydrophilic side chains of the protein or to other water molecules. They are found in the same position in other FABP structures, where they are involved in similar interactions with their respective protein/ligand environments. The tail of the fatty acid is lying against the turn between strands C and D, which probably adopts two conformations in the crystal. This region (together with the αII-helix, Figure 6) is called the portal region, and a conformational flexibility was postulated for this part of the protein to explain entering of the fatty acid into the cavity. Interestingly, instead of a highly conserved phenylalanine, human and ruminant E-FABP contain Leu60 while rodent E-FABP contains Val60 (Figure 5A). This residue is inwardly oriented in *apo*-A-FABP but outwardly oriented in *holo*-A-FABP. Mutations of this portal Phe57 (A-FABP numbering) revealed its importance for the formation of the fatty acid—FABP complex, but did not influence binding selectivity (*49*). Substitution of Phe57 in A-FABP for alanine results in a 3-fold loss of fatty acid binding affinity (*50*).

To conclude, the crystal structure very clearly indicates that E-FABP belongs to the FABP protein structure family. The heterologously expressed functional protein contains one disulfide bridge (for a total of six cysteines), which is unique for an FABP. The eventual importance of this bridge for function cannot be deduced from the crystal structure alone. The recombinant protein clearly has a fatty acid type ligand bound, whose length is between C_{16} and C_{18}. This ligand has a binding mode identical to those observed in A-FABP, B-FABP,[4] H-FABP, and M-FABP that all are members of a subfamily sharing several common features from a structural as well a functional point of view: in these phylogenetically closely related proteins the fatty acid molecule bound adopts a U-shaped conformation and the carboxyl group was calculated to be protonated for A-FABP and H-FABP which might also be the case for the other members of this FABP subfamily addressed above. In addition, near the N-terminus a tyrosine resides within a recognition sequence for phosphorylation by a tyrosine kinase. The phosphorylation of A-FABP and H-FABP is well-documented and the putative meaning for signal transduction events has been discussed (*51*, *52*). Evidence for a phosphorylation of Tyr22 in E-FABP

[3] See UniGene database, on-line available via the following site: http://www.ncbi.nlm.nih.gov/UniGene/.

[4] G. Balendra, G. Scapin, F. Schnütgen, F. Spener, and J. C. Sacchettini, manuscript in preparation.

has also been suggested (*30*). The participation of the members of this particular FABP subfamily in growth inhibition and/or tumor suppression has been recognized on numerous accounts and has recently been reviewed (*53*).

ACKNOWLEDGMENT

This work is part of the Ph.D. thesis of C.H. The authors thank their colleagues from the University of Münster: Dr. Luftmann for GC-MS analyses, B. Schedding for N-terminal protein sequencing, Dr. Lüdemann for MALDI-MS measurements, and Dr. Eicken for helpful introduction to display software.

REFERENCES

1. Hohoff, C., and Spener, F. (1998) *Fett/Lipid 100*, 252−263.
2. Schoonjans, K., Martin, G., Staels, B., and Auwerx, J. (1997) *Curr. Opin. Lipidol. 8*, 159−166.
3. Banaszak, L. J., Winter, N., Xu, Z., Bernlohr, D. A., Cowan, S., and Jones, T. A. (1994) *Adv. Protein Chem. 45*, 89−151.
4. Madsen, P., Rasmussen, H. H., Leffers, H., Honoré, B., and Celis, J. E. (1992) *J. Invest. Dermatol. 98*, 299−305.
5. Siegenthaler, G., Hotz, R., Chatellard-Gruaz, L., Didierjan, L., and Hellman, U. (1994) *Biochem. J. 302*, 363−371.
6. Nordlund, J. J., and Farooqui, J. Z. (1994) U.S. Patent 5,719,-126 (WO 94/12534, PCT/US93/11139).
7. Farooqui, J. Z., Robb, E., Boyce, S. T., Warden, G. D., and Nordlund, J. J. (1995) *J. Invest. Dermatol. 104*, 739−743.
8. Sambrook, J., Fritsch, E. F., and Maniatis, T. (1989) *Molecular Cloning: A Laboratory Manual*, 2nd ed., Cold Spring Harbor Laboratory Press, Plainview, NY.
9. Studier, F. W., Rosenberg, A. H., Dunn, J. J., and Dubendorff, J. W. (1990) *Methods Enzymol. 185*, 60−89.
10. Laemmli, U. K. (1970) *Nature 227*, 680−685.
11. Gill, S. C., and von Hippel, P. H. (1989) *Anal. Biochem. 182*, 319−326.
12. Xu, L. Z., Sanchez, R., Sali, A., and Heintz, N. (1996) *J. Biol. Chem. 271*, 24711−24719.
13. Riddles, P. W., Blakeley, R. L., and Zerner, B. (1983) *Methods Enzymol. 91*, 49−61.
14. Specht, B., Oudenampsen-Krüger, E., Ingendoh, A., Hillenkamp, F., Lezius, A. G., and Spener, F. (1994) *J. Biotechnol. 33*, 259−269.
15. Computational Collaborative Project Number 4 (1994) The CCP4 Suite: Programs for Protein Crystallography. *Acta Crystallogr., Sect. D 50*, 760−763.
16. Navaza, J. (1994) *Acta Crystallogr., Sect. D 50*, 157−163.
17. Zanotti, G., Scapin, G., Spadon, P., Veerkamp, J. H., and Sacchettini, J. (1992) *J. Biol. Chem. 267*, 18541−18550.
18. Roussel, A., and Cambillau, C. (1992) TURBO−FRODO, Biographics, LCCMB, Marseille, France.
19. Otwinowski, Z. (1993) in *Data Collection and Processing. Proceedings of the CCP4 Study Weekend* (Sawyer, L., Isaacs, N., and Bailey, S., Eds.) pp 56−62, SERC Daresbury Laboratory, Warrington, U.K.
20. Brünger, A. (1992) *X-PLOR. Version 3.1 A system for X-ray crystallography and NMR*. Yale University Press, New Haven, CT.
21. Schnütgen, F., Börchers, T., Müller, T., and Spener, F. (1996) *Biol. Chem. Hoppe-Seyler 377*, 211−215.
22. Sacchettini, J. C., and Gordon, J. I. (1993) *J. Biol. Chem. 268*, 18399−18402.
23. Herr, F. M., Aronson, J., and Storch, J. (1996) *Biochemistry 35*, 1296−1303.
24. Xu, Z., Bernlohr, D. A., and Banaszak, L. J. (1993) *J. Biol. Chem. 268*, 7874−7884.
25. Watanabe, R., Fujii, H., Odani, S., Sakakibara, J., Yamamoto, A., Ito, M., and Ono, T. (1994) *Biochem. Biophys. Res. Commun. 200*, 253−259.
26. Wen, Y., Li, G. W., Chen, P., Wong, E., and Bekhor, I. (1995) *Gene 158*, 269−274.
27. Liu, Y., Molina, C. A., Welcher, A. A., Longo, L. D., and De León, M. (1997) *J. Neurosci. Res. 48*, 551−562.
28. Krieg, P., Feil, S., Fürstenberger, G., and Bowden, T. G. (1993) *J. Biol. Chem. 268*, 17362−17369.
29. Bernlohr, D. A., Coe, N. R., Simpson, M. A., and Hertzel, A. V. (1997) *Adv. Exp. Med. Biol. 422*, 145−156.
30. Jaworski, C., and Wistow, G. (1996) *Biochem. J. 320*, 49−54.
31. Kingma, P. B., Bok, D., and Ong, D. E. (1998) *Biochemistry 37*, 3250−3257.
32. Thornton, J. M. (1981) *J. Mol. Biol. 151*, 261−287.
33. Richardson, J. (1981) *Adv. Protein Chem. 34*, 167−339.
34. Kane, C., Coe, N., Vanlandingham, B., Krieg, P., and Bernlohr, D. A. (1996) *Biochemistry 35*, 2894−2900.
35. Kleywegt, G. J., and Jones, T. A. (1994) *Acta Crystallogr., Sect. D 50*, 178−185.
36. Cowan, S. W., Newcomer, M. E., and Jones, T. A. (1993) *J. Mol. Biol. 230*, 1225−1246.
37. Lalonde, J., Bernlohr, D. A., and Banaszak, L. J. (1994) *Biochemistry 33*, 4885−4895.
38. Scapin, G., Gordon, J. I., and Sacchettini, J. C. (1992) *J. Biol. Chem. 267*, 4253−4269.
39. Woolf, T. B. (1998) *Biophys. J. 74*, 681−693.
40. Börchers, T., and Spener, F. (1994) *Curr. Top. Membr. 40*, 261−294.
41. Kitamura, K., Suzuki, M., Suzuki, A., and Uyemura, K. (1980) *FEBS Lett. 115*, 27−30.
42. Tenchini, M. L., Morra, F., Soranzo, C., and Malcovati, M. (1995) *Epithelial Cell Biol. 4*, 143−155.
43. Brodersen, D. E., Etzerodt, M., Madsen, P., Celis, J. E., Thogersen, H. C., Nyborg, J., and Kjeldgaard, M. (1998) *Structure 6*, 477−489.
44. Raftery, M. J., Harrison, C. A., Alewood, P., Jones, A., and Geczy, C. L. (1996) *Biochem. J. 316*, 285−293.
45. Vorum, H., Brodersen, R., Kragh-Hansen, U., and Pedersen, A. O. (1992) *Biochim. Biophys. Acta 1126*, 135−142.
46. Vorum, H., Madsen, P., Svendsen, I., Celis, J. E., and Honoré, B. (1998) *Electrophoresis 19*, 1793−1802.
47. Scapin, G., Young, A. C., Kromminga, A., Veerkamp, J. H., Gordon, J. I., and Sacchettini, J. C. (1993) *Mol. Cell. Biochem. 123*, 3−13.
48. Thompson, J., Winter, N., Terwey, D., Bratt, J., and Banaszak, L. (1997) *J. Biol. Chem. 272*, 7140−7150.
49. Simpson, M. A., and Bernlohr, D. A. (1998) *Biochemistry 37*, 10980−10986.
50. Richieri, G., Low, P., Ogata, R., and Kleinfeld, A. (1998) *J. Biol. Chem. 273*, 7397−7405.
51. Hresko, R. C., Hoffman, R. D., Flores-Riveros, J. R., and Lane, M. D. (1990) *J. Biol. Chem. 265*, 21075−21085.
52. Nielsen, S. U., and Spener, F. (1993) *J. Lipid Res. 34*, 1355−1366.
53. Hohoff, C., and Spener, F. (1998) *Cancer Res. 58*, 4015−4017.
54. Ong, D. E., Newcomer, M. E., and Chytil, F. (1994) in *The Retinoids: Biology, Chemistry, and Medicine* (Sporn, M. B., Roberts, A. B., and Goodman, D. S., Eds.) pp 283−317, Raven Press, New York.
55. Page, R. D. (1996) *Comput. Appl. Biosci. 12*, 357−358.
56. Santomé, J. A., Di Pietro, S. M., Cavagnari, B. M., Cordoba, O. L., and Dell′Angelica, E. C. (1998) *Trends Comp. Biochem. Physiol. 4*, 23−38.

BI990305U